Development of LaMnO$_3$ and LaNiO$_3$ type materials with calcium doping by the modified proteic method and evaluation for the dye removal efficiency

A. A. Souza[1], J. B. R. Fernandes[2], J. F. S. Ribeiro[1], M. J. B. Souza[3]*, A. M. Garrido Pedrosa[1,2]
[1]Federal University of Sergipe, Graduate Program in Chemistry, São Cristóvão, SE, Brazil
[2]Federal University of Sergipe, Department of Chemistry, São Cristóvão, SE, Brazil
[3]Federal University of Sergipe, Department of Chemical Engineering,
Av. Mal. Rondon, 49100-000, São Cristóvão, SE, Brazil

Abstract

Materials by the modified proteic method based on calcium doped LaMnO$_3$ and LaNiO$_3$, with perovskite structure were prepared. The X-ray diffraction patterns revealed the presence of the perovskite phase in all materials, whose specific surface area values varied between 27 and 37 m^2.g^{-1}. The materials presented efficiency for the removal of Congo red dye and those with site B occupied by nickel presented better adsorptive efficiency. The incorporation of calcium on LaMnO$_3$ or LaNiO$_3$ materials caused an improvement in the performance of the materials for the dye removal from water. The materials maintained perovskite structure after the adsorption tests, allowing their reuse in new adsorption tests with high efficiency.
Keywords: LaMnO$_3$, LaNiO$_3$, calcium, modified proteic method, dye removal.

INTRODUCTION

Environmental pollution is a problem of modern society, and the textile industry, for example, during dyeing processes releases dyes that are hardly naturally degraded, requiring wastewater treatment [1]. Adsorption is one the way to remove dyes and has gained prominence as it is an efficient, simple, and economical technique [2, 3]. Among several adsorbents used for this purpose, metal oxides have shown to be efficient adsorbents [2-5], because, among so many properties that enhance their use, in general, they have porous structures, metallic sites in their structures that can interact with the dye structure, and due to their stability there is the possibility of their recovery after application and reuse [2, 5]. The interaction of the dye with metal oxide used as adsorbents can involve electrostatic interactions such as ionic interaction, van der Waals forces, hydrogen bonds, and covalent bonds. Depending on the adsorbent-adsorbate system, one or more forces act on the process [5].

LaMnO$_3$ and LaNiO$_3$ materials are oxides that present good thermal and chemical stability and are ceramic materials with perovskite structure; materials with this structure have a variety of applications [6-18], such as in catalysis [7, 9, 11, 13, 16], SOFC electrode [7, 8], magnetic sensors [7, 8, 15], capacitors [7, 8, 14], and adsorption of dyes [12]. These ceramic materials have been studied as efficient catalysts for several reactions being mechanically and chemically stable under drastic reaction conditions.

The properties of materials with perovskite structure can still be manipulated by partially substituting at its metallic sites for metals of different oxidation states [9, 11, 14, 16]. The incorporation of calcium in materials such as LaMO$_3$ (M= Mn, Ti) in which La^{3+} sites are partially replaced by Ca^{2+} ions in the crystalline network may affect some of their properties of technological interest, resulting in materials with optimized properties [14, 16, 17]. These diverse possibilities of applications of ceramic materials with a perovskite structure have increased interest in new ways of obtaining these materials or improving existing methods, considering that these properties are potentially influenced by the synthesis method that can generate materials with great potential for an application and low-cost. The protein method or protein gel is an alternative, low-cost, and less aggressive route to the environment to produce ceramic materials [9, 18, 19]. In this chemical route, the formation of the oxide occurs due to the complexation of the chelating agent with metallic cations, as well as by the conventional methods of Pechini, chelating precursors, and polymeric precursors. However, in the modified protein method, the chelating agent is replaced by a substance with high protein content, such as gelatin, soy, or collagen so that the reaction proceeds with fewer steps, as the interaction occurs directly with the amino acids in the protein composition. In addition, the temperatures typically required to obtain the crystalline phase are generally lower [9, 18, 19].

In the present study, the synthesis of LaMnO$_3$ and LaNiO$_3$ type materials with calcium doping by the modified proteic method is presented and their use as an adsorbent for dye removal is evaluated, besides verifying the possibility of recovery and reuse of these materials. Studies using

* *marcelojbs@ufs.br*
https://orcid.org/0000-0001-6703-1547

oxides with perovskite structure for this application are still relatively few, as well as the preparation of materials by this method.

EXPERIMENTAL

Synthesis of the materials: $LaMO_3$ and $La_{0.5}Ca_{0.5}MO_3$ materials (M= Ni or Mn) were synthesized by the modified proteic method adapted from the literature [9, 18, 19] and using nickel nitrate II hexahydrate (Vetec, 97.0%), manganese nitrate II tetrahydrate (Neon, 98.8%), lanthanum nitrate III hexahydrate (JT Baker, 99.9%), calcium nitrate tetrahydrate (Synth, 99.0%), and collagen (Nutrigold) as a metal complexing agent. The synthesis procedures for obtaining materials without doping ($LaNiO_3$ and $LaMnO_3$) and with doping ($La_{0.5}Ca_{0.5}MnO_3$ and $La_{0.5}Ca_{0.5}NiO_3$) were similar with a difference only at the time of addition of the doping material precursor (calcium nitrate tetrahydrate). For the synthesis of the materials, the reagent of the cation that should occupy site B of perovskite (manganese nitrate or nickel nitrate) was dissolved in 100 mL of distilled water under magnetic stirring at 100 rpm, at 30 °C for 30 min. Then a stoichiometric mass of lanthanum nitrate was added to the system, keeping the system under stirring at the same temperature for a further 30 min. Subsequently, the system temperature was raised to 70 °C and upon stabilization, collagen was added and the system was stirred for more 1.5 h at 70 °C. For the synthesis of doped materials, the experimental procedure was similar, but together with the addition of the lanthanum nitrate mass, the stoichiometric mass of calcium nitrate was added. The resultant system was pre-calcined in a muffle furnace at a heating rate of 10 °C.min^{-1} until it reached 350 ºC, where it remained for 2 h, forming the precursor powder. The material obtained was ground and calcined at a heating rate of 10 ºC.min^{-1} in a muffle furnace until reaching 900 ºC, where it remained for 2 h. The calcined materials were named LM9-C, LN9-C, L5C5M9-C, and L5C5N9-C for $LaMnO_3$, $LaNiO_3$, $La_{0.5}Ca_{0.5}MnO_3$, and $La_{0.5}Ca_{0.5}NiO_3$, respectively.

Characterizations of the materials: the X-ray diffraction (XRD) patterns of the calcined materials at 900 ºC were obtained using a diffractometer (Panalytical) with CuKα radiation (λ=1.5406 Å), 2θ in the range of 10º to 60º, and a scanning speed of 5 °.min^{-1}. For identification of the crystalline structure, the obtained XRD patterns were compared with the JCPDS and ICDD database. The mean crystallite size was calculated from the three main peaks of the perovskite phase [9, 18, 20] and using Scherrer's equation. The specific surface areas of the materials were determined via nitrogen adsorption at 77 K (NOVA 1200e, Quantachrome) employing about 100 mg of each sample calcined at 900 °C. The samples were previously degassed at 300 °C for 1 h in order to remove any species on the sample surface and then subjected to analysis. An isotherm with nine adsorption points was obtained in the relative pressure range between 0.05 and 0.99, and the specific surface area was calculated using the BET method, in the range of values

of relative pressure between 0.05 and 0.30. The pH at the point of zero charge (pH_{pcz}) was determined using 20 mg of each material (calcined at 900 °C) and 20 mL of the previously prepared 0.10 mol.L^{-1} NaCl solution, with pH values adjusted from 1 to 11 using NaOH or HCl solutions at 10 and 0.05 mol.L^{-1}, respectively. The systems were stirred at 23 °C for 1 h on a magnetic stirrer (Gostirrer), and after the samples were filtered with a qualitative filter paper the final pH of the solutions was measured with a benchtop pH meter (Micronal). The pH_{pcz} values were determined based on the method proposed by Smiciklas et al. [21].

Adsorption tests: prior to the adsorption tests, Congo red dye aqueous solution was prepared at 34 mg.L^{-1} and analyzed on UV-vis region with a spectrophotometer (UV-1800, Shimadzu) using a quartz cell of 3.5 mL with 1.0 cm optical path, and scanning at a wavelength range of 200 to 700 nm. An analytical curve was obtained. The adsorption experiments were conducted under magnetic stirring at 150 rpm, at 25 ºC and in some established times an aliquot of the supernatant was withdrawn, filtered, and analyzed by absorption spectrophotometry in the UV-vis region under the same conditions used in the reference solution. During the adsorption assays, the materials used (LM9-C, LN9-C, L5C5M9-C, and L5C5N9-C) were previously dried at 60 ºC for 30 min, then the mass of 100 mg was used. The tests were conducted in triplicate. Besides this, in adsorption studies, the pH of the dye solution was measured at the beginning and the end of the assay and kept constant at pH 5, which was the pH of the reference solution. The light effect (photolysis) without the presence of adsorbent on dye degradation was also studied with Congo red dye aqueous solution at 34 mg.L^{-1}. The study was done to assess whether the dye solution was stable under the experimental conditions of the adsorption tests (laboratory light, temperature, degree of agitation), but in the absence of the adsorbent. Adsorption efficiency (E%) and amount of adsorbed dye in mg/g of adsorbent (q) were calculated based on equations reported in the literature [12, 18]. The pseudo-first-order and pseudo-second-order models were used to study the adsorption kinetics [22]. After adsorption tests, the materials retained in the filter papers were oven-dried at 80 °C for 1 h and part of it was subjected to X-ray diffraction and another part was calcined at 900 °C for 2 h for the dye degradation and to the adsorbent recovery. The adsorbent reuse tests were conducted similarly to that described previously for adsorption tests, except the sampling time of the supernatant aliquot that was the last experimental time.

RESULTS AND DISCUSSION

Fig. 1a shows X-ray diffraction patterns for all materials synthesized and Fig. 1b for recovered materials after adsorption tests. The XRD patterns for the materials LM9-C and L5C5M9-C showed peaks related to the $LaMnO_3$ and $La_{0.5}Ca_{0.5}MnO_3$ perovskite phase, at 2θ= 22.93°, 32.49°, 32.70°, 40.63°, 46.81°, 52.56°, and 58.12° in both materials, but besides these peaks, the material LM9-C also presented
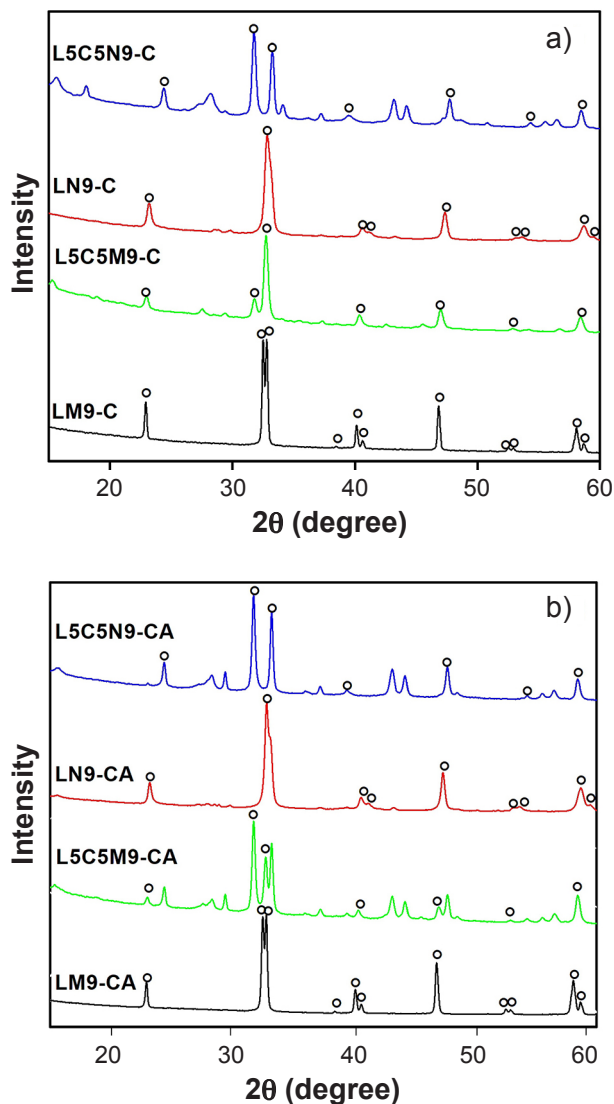
Figure 1: X-ray diffraction patterns of the as-synthesized materials (a) and materials after the adsorption test (b) (° - perovskite phase).

the peaks referring to the perovskite structure at $2\theta= 38.46°$, $40.17°$, $53.01°$, and $58.70°$ (JCPDS 32-0485). $LaMnO_3$ perovskite was the only phase presented in the material LM9-C, indicating the efficiency of the synthesis method and conditions used. Calcium-doped material (L5C5M9-C) also presented secondary phases, with peaks at $2\theta= 27.51°$, $29.39°$, and $37.39°$ due to the La_2O_3 phase (JCPDS 83-1355). XRD patterns of LN9-C and L5C5N9-C materials presented peaks related to the perovskite phase $LaNiO_3$ and $La_{0.5}Ca_{0.5}NiO_3$, respectively, at $2\theta= 23.19°$, $32.82°$, $40.69°$, $47.34°$, $53.64°$, and $58.72°$, but the peaks at $2\theta= 41.13°$, $53.18°$, and $59.41°$ appeared only for the material LN9-C and at $2\theta=31.77°$ in the doped material (L5C5N9-C). The perovskite phases had a rhombohedral structure (JCPDS 33-0711). The nickel-based materials showed few peaks due to the secondary phases, such as NiO (JCPDS 44-1159) and La_2O_3 (JCPDS 83-1355). These were the common phases for both materials, but the doped material presented another secondary phase,

which was identified as CaO with a peak at $2\theta=37.21°$ (JCPDS 37-1497).

Manganese-based materials had more distorted structures than nickel-based materials, compared to the ideal cubic geometry of the perovskite. This difference can be explained by the difference in ion size, Mn^{3+} (65 pm) that is larger than Ni^{3+} (60 pm), which caused distortions in the crystal structures, altering the length of the B-O bond, thereby distorting the octahedron BO_6 of the perovskite structure ABO_3 (B= Ni, Mn) [7]. Differences were also noted when comparing the materials without doping with their materials partially replaced by the Ca^{2+} ion (with doping). It was possible to observe the shift of some lower intensity peaks corresponding to the perovskite structure. The Ca^{2+} ion (99 pm) has an ionic radius smaller than the La^{3+} metal ion (103 pm), so the doped materials $La_{0.5}Ca_{0.5}NiO_3$ and $La_{0.5}Ca_{0.5}MnO_3$ presented the ionic radii of their A sites less than the ionic radii of the A sites for $LaMnO_3$ and $LaNiO_3$ materials without doping. This decrease in radius caused changes in the angles of the octahedron B-O bonds (B= Ni or Mn), decreasing the cell volume and increasing the diffraction angles, as well as decreasing the intensity of some peaks of the perovskite phase [7, 17]. The sample L5C5N9-C presented more secondary phases than other samples, possibly as a consequence of the presence of divalent ion (Ca^{2+}) and due to the ion Ni^{4+} is not as stable as the ion Mn^{4+}. According to the literature [9, 10, 19], partial substitution causes a nickel charge imbalance in Ni^{2+} and Ni^{3+}, consequently, there is the formation of oxygen vacancies and the production of secondary phases or a mixture of oxidation states in the perovskite, compensated by non-stoichiometry of oxygen.

The results of the average size of crystallites and specific surface area are shown in Table I. The crystallites had an average size between 11 and 43 nm, and it was noted that the material LM9-C presented a significantly larger crystallite size than the other crystallites, but there was coherence between the results and data in the literature [9, 19]. On the other hand, the specific surface area (SSA) values were relatively larger than typically reported in the literature [14, 23]. The SSA values for LM9-C and L5C5M9-C materials were 27 and 35 $m^2.g^{-1}$, respectively. Nickel-based materials had surface areas of 31 and 37 $m^2.g^{-1}$ for LN9-C and L5C5N9-C, respectively, and the literature shows a relatively smaller surface area for the $LaNiO_3$ perovskite (3.15 $m^2.g^{-1}$) synthesized by the sol-gel method [14]. The surface area of the doped materials increased in relation to the respective materials without doping probably due to the presence of XRD-confirmed secondary phases. Partial replacement of the La^{3+} ion with a smaller ion (Ca^{2+}) caused the electronic charge imbalance [9, 14]. In a recent study, a 30% strontium-doped $LaNiO_3$ perovskite had a surface area of 26 $m^2.g^{-1}$, and with 70% strontium occupying site A (La) of the $LaNiO_3$ perovskite had 38 $m^2.g^{-1}$, confirming that partial replacement of the perovskite sites may increase the surface area, probably due to electronic imbalance [9]. Table I shows the pH at the point of zero charge (pH_{pcz}) for

the materials. The point of zero charge (pcz) for the LM9-C and LN9-C materials was approximately pH 7, whereas for L5C5M9-C and L5C5N9-C materials it was approximately pH 9. The Congo red dye is an anionic dye, which adsorption is favored when the adsorbent contacts a liquid solution with a pH lower than pcz, when an electrostatic attraction between the positive ions from the metals of perovskite structure and the negatively charged groups from the dye occurs [5].

Table I - Mean crystallite size (D), specific surface area determined by BET method (S_{BET}), and pH at the point of zero charge (pH_{pcz}) of synthesized materials.

Material	D (nm)	S_{BET} (m².g⁻¹)	pH_{pcz}
LM9-C	43	27	7.4
L5C5M9-C	11	35	9.5
LN9-C	15	31	7.3
L5C5N9-C	16	37	9.2

In order to evaluate the potential of prepared materials as dye adsorbent, the removal of the Congo red dye from the aqueous medium was studied. First, it was evaluated if under the study conditions the dye underwent photodegradation under the effect of light and agitation (without the adsorbent). The test using the stock solution was subjected to magnetic stirring at ambient light, and aliquots at fixed times were withdrawn and analyzed by UV-vis spectrophotometry. Its difficult degradation was noted as there was no change in UV-vis spectra and it was found that the Congo red dye is not photodegradable (Fig. 2). The adsorption kinetics was performed in order to verify the adsorptive capacities of materials ($La_{0.5}Ca_{0.5}NiO_3$, $La_{0.5}Ca_{0.5}MnO_3$, $LaNiO_3$, and $LaMnO_3$) in the removal of Congo red dye from the aqueous medium and the effect of calcium doping in the efficiency. Fig. 3 shows the adsorption efficiency values (E%) for LM9-C, LN9-C, L5C5M9-C, and L5C5N9-C materials. The efficiencies ranged from 82% to 94% and nickel-based materials proved to be better adsorbents. The higher efficiency of the nickel-based materials may be related to the crystallite size and surface area, since the crystallite of the LN9-C material was 15 nm and its surface area was 31 m².g⁻¹ while the crystallite size for the material LM9-C was 43 nm and the surface area was 27 m².g⁻¹. On the other hand, L5C5M9-C material had 11 nm crystallite size, while L5C5N9-C had 16 nm crystallite size, but nickel-based material had a larger surface area even though its crystallite was slightly larger than the base manganese-doped material. Therefore, the results indicated that materials with larger surface areas optimize adsorption. Moreover, the crystallite sizes of both were small and close, as well as the adsorption efficiency which was 94% for L5C5N9-C and 92% for L5C5M9-C.

The most noticeable differences were between the no doping and partial doping materials, whose efficiencies were 82% and 92% for LM9-C and L5C5M9-C, respectively, and 87% and 94% for LN9-C and L5C5N9-C, respectively. It
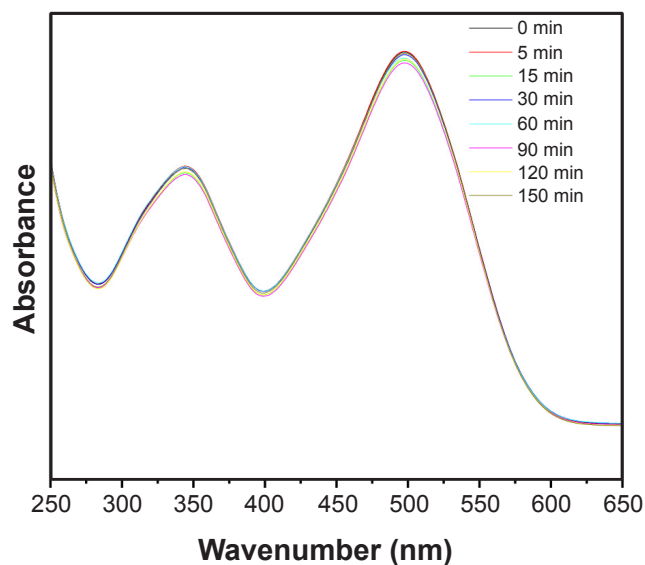

Figure 2: UV-vis spectra of Congo red dye solution at different times of agitation.
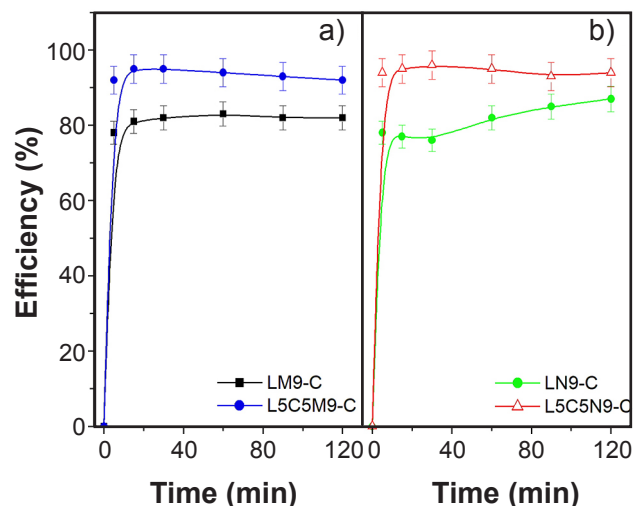

Figure 3: Efficiency of Congo red dye removal using manganese-based materials (a) and nickel-based materials (b).

was noted that Ca^{2+} ion insertion in the material significantly improved adsorbent activity, indicating that by partially replacing site A ions with other lower valence cations, such as the substitution of La^{3+} with Ca^{2+}, oxygen vacancies are formed, which can contribute to the adsorption ions and move across the surface of the material, promoting interaction between species [14, 19, 24]. The material L5C5N9-C was the best adsorbent even without the smallest crystallite, but it was the material that presented the largest surface area and this fact can be explained by the imbalance of nickel charges in Ni^{2+} and Ni^{3+} when partially replaced by Ca^{2+}. Doping may promote the formation of oxygen vacancies and the production of secondary phases or a mixture of oxidation state in the perovskite, compensated by non-stoichiometry of oxygen, making porous material an important feature for an adsorbent [2, 6, 14, 16]. In general, metal oxides are efficient

adsorbents due, among many factors, to the presence of Lewis acid and base type sites, oxygen vacancies, and consequently structural defects [2, 5].

Fig. 4 shows the experimental values of the adsorption assays and the values found by the pseudo-first-order (PFO) and pseudo-second-order (PSO) models; in addition, Table II shows the parameters obtained for the adsorption kinetics of Congo red in different materials. It was noted that the two models applied were consistent with the experimental data, presenting very similar quantities of adsorbed dye. The results suggested that the model that best fitted the experimental data was the pseudo-first-order model since it was closer to the experimental values and had a smaller error. However, the parameters presented by regression to the PSO model indicated that this model can also be system representative. The models also allowed the determination of velocity constants k_1 for pseudo-first-order and k_2 for pseudo-second-order. It was noted that the dye removal kinetics was faster when using the adsorbents that

contained the calcium ion compared to the adsorbents that did not contain it. The velocity was higher for the doped materials, agreeing that they were the best adsorbents and this agreement was indicative that the doped materials had better interaction with the Lewis bases present in the dye [5, 15]. It is suggested that there was a coordination between the cations of the perovskite structure with electron-donating groups present in dye structure: $(SO_3)^-$, NH_2, and $N=N$ [5, 12, 16, 18]. Then, as the calcium-containing samples showed higher adsorption efficiency, it is suggested that these adsorbents have a higher specificity for adsorption of Congo red than undoped materials.

Because it is a relatively simple technique, the use of adsorption for the removal of pollutants is constantly increasing, for example in the removal of dyes [5, 24-28]. Table III shows some results reported in the literature regarding the adsorption capacity of different materials in the removal of Congo red dye from the aqueous medium. For comparative purposes, almost all exposed adsorbents
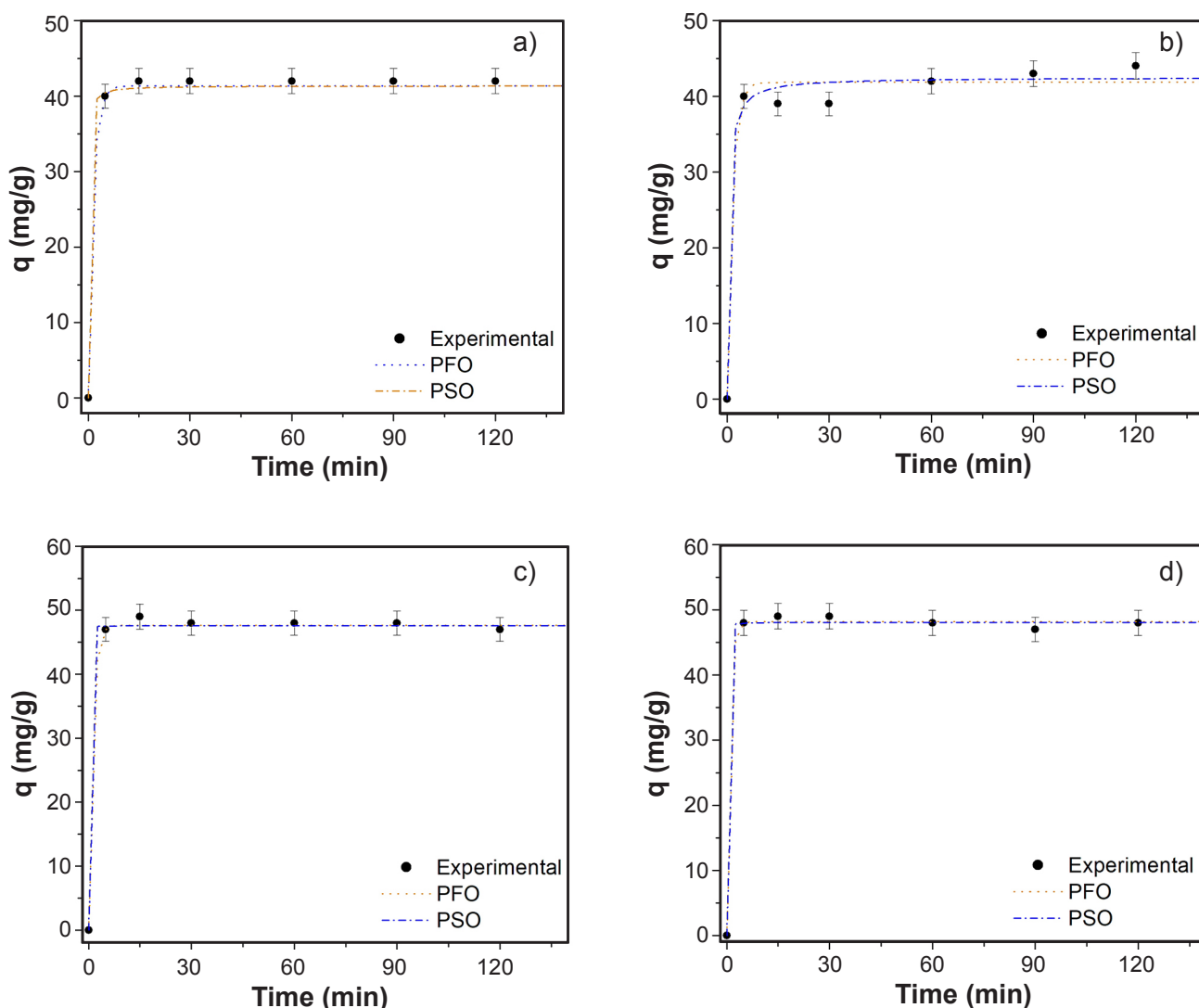

Figure 4: Adsorption kinetics of Congo red dye on the materials: a) LM9-C; b) LN9-C; c) L5C5M9-C; and d) L5C5N9-C (PFO: pseudo-first-order; PSO: pseudo-second-order).

Table II - Parameters obtained by the pseudo-first-order (PFO) and pseudo-second-order (PSO) models for the adsorption kinetics of Congo red in different materials.

Material	q (mg.g^{-1})	k$_1$ (min^{-1})	R^2	χ^2
		PFO		
LM9-C	41.33±0.61	0.69±0.24	0.9911	0.2225
LN9-C	41.84±0.86	0.62±0.25	0.9826	0.4688
L5C5M9-C	47.66±0.38	0.85±0.31	0.9973	0.8889
L5C5N9-C	48.17±0.28	1.13±0.60	0.9986	0.4722
		PSO		
LM9-C	41.36±0.73	0.22±0.16	0.9905	0.3779
LN9-C	42.50±0.89	0.05±0.03	0.9868	0.3805
L5C5M9-C	47.58±0.46	3.69±0.78	0.9971	0.9520
L5C5N9-C	48.07±0.33	1.53±0.97	0.9985	0.4988

showed adsorption capacity close to the results obtained from the adsorption capacity in the present work. Such results reinforced the feasibility of using the studied materials to remove dyes, especially Congo red. The ZnO adsorbent synthesized by homogeneous precipitation (CZ-400) was efficient to remove Congo red dye, removing 10.2 mg.g^{-1} when the initial dye concentration was 50 mg.L^{-1} and 97 mg.g^{-1} when the initial concentration of dye was 200 mg.L^{-1} [25]. An adsorbent obtained from bamboo sawdust was used for adsorption of Congo red dye from an aqueous solution kept under stirring for 12 h; the maximum dye removal was 33.7 mg.g^{-1} [26].

The search for adsorbents that are not only efficient but can also be reused is continuous. In order to evaluate the possibility of recovery of the studied adsorbents, it was verified if the structures of the adsorbents were maintained after the adsorption tests. Through the information obtained, it was possible to analyze if these materials can be recovered and reused as adsorbents; if feasible, the formation of new residues and new costs is avoided. Fig. 1b shows the X-ray diffractograms of the recovered materials. The samples LM9-CA, L5C5M9-CA, LN9-CA, and L5C5N9-CA refer to materials LM9-C, L5C5M9-C, LN9-C, and L5C5N9-C,

respectively, after use in the adsorption test and drying in an oven at 80 °C for 1 h. Analyzing the XRD patterns, it was seen that the perovskite structure remained in all materials after the adsorption tests since all peaks concerning the structure were maintained. In addition, all secondary phases were also preserved, but for the material L5C5N9-CA, there was the absence of peaks referring to La$_2$O$_3$ and NiO, present before adsorption. In addition, all the XRD patterns had as a common characteristic the increase in the intensity of their peaks when compared with their XRD patterns before the adsorption test. After verifying that the perovskite structure was maintained in all materials after the adsorption tests, they were recovered and subjected to new adsorption tests, and thus it was possible to compare the adsorptive performance of the materials in both uses, as shown in Fig. 5. The adsorption performances of the materials LM9-C and L5C5M9-C remained practically the same, that is, their second use was little compromised by the first adsorption performances, indicating perhaps greater stability of these materials. Nickel-based materials showed a small difference in their two uses. LN9-C had an increase in the second use, unlike material L5C5N9-C. This difference can be attributed to the experimental error, but it may also have had

Table III - Absorption capacity of Congo red dye using various materials as adsorbents and experimental conditions.

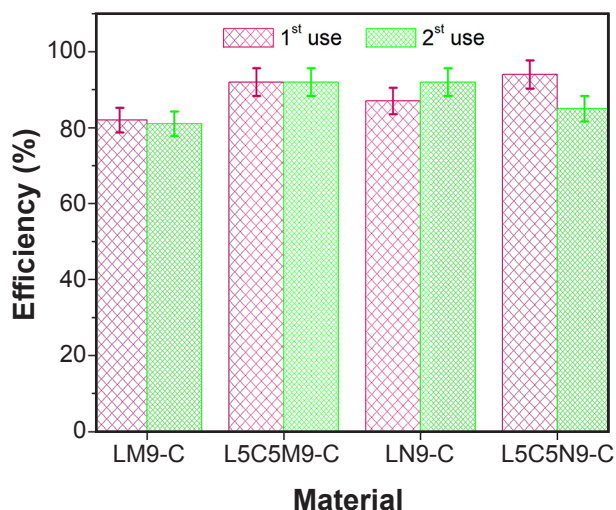| Material	Mass of adsorbent/ Solution volume	pH	C (mg.L^{-1})	Q (mg.g^{-1})	Ref.
Fe$_{2.95}$La$_{0.05}$O$_4$	15 mg/50 mL	5.5	30	28.5	[27]
Jute stick powder	500 mg/50 mL	6.0-7.0	50	35.7	[28]
ZnO	40 mg/20 mL	7.0	50	10.2	[25]
Bamboo hydrochars	100 mg/50 mL	-	100	33.7	[26]
LM9-C	100 mg/150 mL	5.0	34	42.0	This work
LN9-C	100 mg/150 mL	5.0	34	44.0	This work
L5C5M9-C	100 mg/150 mL	5.0	34	47.0	This work
L5C5N9-C	100 mg/150 mL	5.0	34	48.0	This work

Figure 5: Adsorption efficiency for dye removal for 1st use and 2nd use of the materials.

contributions from other factors, considering that L5C5N9-C material showed more peaks relative to secondary phases than L5C5M9-C material, which may have influenced the first use in dye removal. After first use, some of these secondary phase peaks disappeared into nickel-doped material due to flattening caused by the presence of very intense perovskite peaks and this may have compromised their second use in dye removal and contributed to the decrease in dye removal.

The influence of calcium doping in the $LaMnO_3$ and $LaNiO_3$ materials on the characteristics (mean crystallite size and specific surface area) and performance of the adsorbents [adsorption efficiency for 1st use (E1) and 2nd use (E2)] are shown in Fig. 6. The calcium loading of 50 shown in Fig. 6 refers to the theoretical substitution percentage of lanthanum for calcium at site A of the perovskite structure. It can be noted that the doping of calcium in the $LaMnO_3$ and $LaNiO_3$ materials improved the characteristics of the material and consequently their efficiency for adsorption of Congo red dye in the first and second use of the adsorbents, with the exception of the second use of L5C5N9-C material. The small decrease in the adsorption efficiency of the dye in the second use of the L5C5N9-C material in relation to the first use can be correlated to the experimental error, but it can also be a consequence of the recrystallization of the material with the disappearance of some secondary phases that also contributed to the removal of the dye, as seen in the X-ray diffraction pattern shown in Fig. 1b. Several materials can be used as adsorbents and the higher the adsorptive capacity and stability of the material, allowing its recovery and reuse, the more attractive the material. In addition, the material synthesis route is also an important factor, when simple and more economical routes are used. This study confirmed the efficiency of dye removal and the stability of the $LaMnO_3$ or $LaNiO_3$ type materials with calcium doping, with perovskite structure, and even under specific recovery conditions, they can be reutilized. During the recovery of the adsorbent, the dye is degraded, as noted in previous studies [12], and from its degradation, several products can potentially be obtained
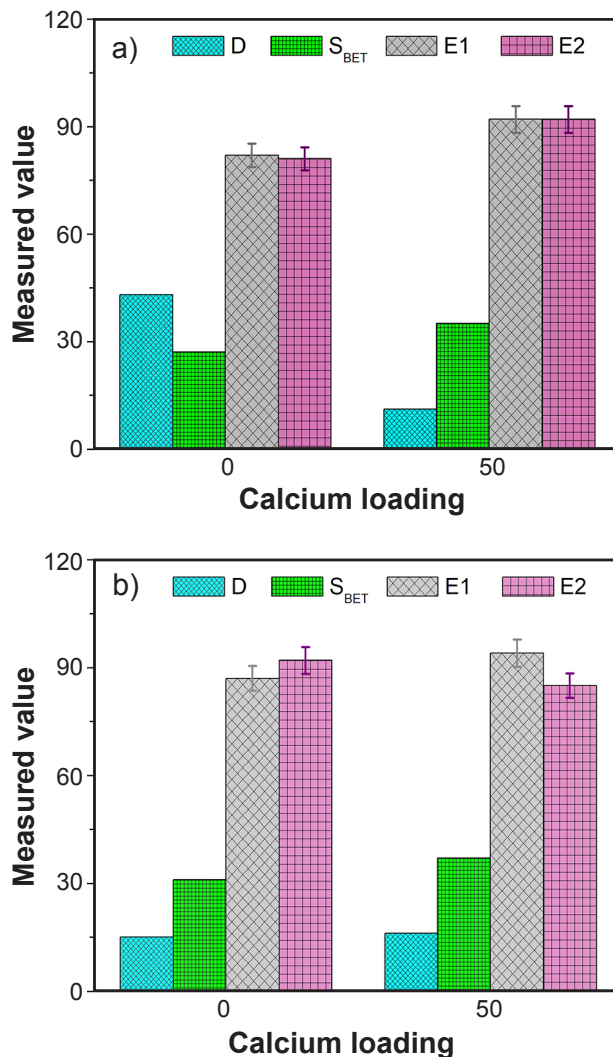

Figure 6: Influence of calcium doping on the characteristics and performance of $LaMnO_3$ (a) and $LaNiO_3$ (b) materials (D: mean crystallite size; S_{BET}: specific surface area, E: adsorption efficiency).

[29], which could be used as fuel for example, although studies still need to be carried out in this regard.

CONCLUSIONS

The modified proteic method is a simple and effective method to obtain $LaMnO_3$ or $LaNiO_3$ type materials with calcium doping and perovskite structure. All materials studied were efficient in the removal of Congo red dye, with efficiency values between 82% and 94% and an amount of adsorbed dye (q) between 38 and 48 $mg.g^{-1}$ of adsorbent. Partial replacement of La^{3+} by lower valence Ca^{2+} cation in $LaMnO_3$ or $LaNiO_3$ influenced the efficiency of dye removal. Calcium doping improved adsorbent efficiency since efficiencies were 82% and 92% for $LaMnO_3$ and $La_{0.5}Ca_{0.5}MnO_3$, and 87% and 94% for $LaNiO_3$ and $La_{0.5}Ca_{0.5}NiO_3$, respectively. Nickel-based materials were slightly better at removing the dye than manganese-based materials; on the other hand, manganese-based materials maintained the dye removal efficiency in the reuse tests,

while in the nickel-based materials the values decreased. The perovskite structure was stable during the adsorption and calcination tests, and its reuse as the adsorbent can be performed considering that the efficiency of Congo red dye removal was practically maintained.

ACKNOWLEDGEMENTS

REFERENCES

[1] J.C. Cardoso, G.G. Bessegato, M.V.B. Zanoni, in "Corantes: caracterização química, toxicológica, métodos de detecção e tratamento", M.V.B. Zanoni, H. Yamanaka (Orgs.), Cultura Acad., São Paulo (2016) 215.
[2] M.T. Yagub, T.K. Sen, S. Afroze, H.M. Ang, Adv. Colloid Interface Sci. **219** (2014) 172.
[3] N. Yahya, F. Aziz, N.A. Jamaludin, M.A. Mutalib, A.F. Ismail, W.N.W. Salleh, J. Jaafar, N. Yusof, N.A. Ludin, J. Environ. Chem. Eng. **6** (2018) 7411.
[4] H. Liu, Z. Wang, H. Li, H. Wang, R. Yu, Mater. Res. Bull. **100** (2018) 302.
[5] M. Nagpal, R. Kakkar, Sep. Purif. Technol. **211** (2019) 522.
[6] H. Chen, J. Motuzas, W. Martens, J.C.D. Costa, Appl. Catal. B **221** (2018) 691.
[7] C. Moure, O. Peña, Prog. Solid State Chem. **43** (2015) 123.
[8] E.C.C. Souza, R. Muccillo, Mater. Res. **13** (2010) 385.
[9] E.O. Moraes Júnior, J.O. Leite, A.G. Santos, M.J.B. Souza, A.M. Garrido Pedrosa, Cerâmica **64**, 371 (2018) 436.
[10] D.J. Deka, S. Gunduz, T. Fitzgerald, J.T. Miller, A.C. Co, U.S. Ozkan, Appl. Catal. B **248** (2019) 487.
[11] F. Magalhães, F.C.C. Moura, J.C. Ardisson, R.M. Lago, Mater. Res. **11** (2008) 307.
[12] A.G. Santos, J.O. Leite, I.F. Gimenez, M.J.B. Souza, A.M. Garrido, Mater. Res. Express **6** (2019) 105065.
[13] R. Gade, J. Ahemed, K.L. Yanapu, S.Y. Abate, Y. Tao, S. Pola, J. Environ. Chem. Eng. **6** (2018) 4504.
[14] T. Tabari, D. Singh, A. Calisan, A. Ebadi, H. Tavakkoli, B. Caglar, Ceram. Int. **43** (2017) 15970.
[15] A. Ashok, A. Kumar, R.R. Bhosale, F. Almomani, S.S. Malik, S. Suslov, F. Tarlochan, J. Electroanal. Chem. **809** (2018) 22.
[16] M. Bradha, T. Vijayaraghavan, S.P. Suriyaraj, R. Selvakumar, A.M. Ashok, J. Rare Earths **33** (2015) 160.
[17] H. Mo, H. Nan, X. Lang, S. Liu, L. Qiao, X. Hu, Ceram. Int. **44** (2018) 9733.
[18] A.G. Santos, J.O. Leite, M.J.B. Souza, I.F. Gimenez, A.M. Garrido Pedrosa, Ceram. Int. **44** (2018) 5743.
[19] F.S. Oliveira, P.M. Pimentel, R.M.P.B. Oliveira, D.M.A. Melo, M.A.F. Melo, Mater. Lett. **64** (2010) 2700.
[20] H. Tavakkoli, M. Yazdanbakhsh, Microp. Mesop. Mater. **176** (2013) 86.
[21] I.D. Smiciklas, S.K. Milonic, P. Pfendt, S. Raicevic, Sep. Purif. Technol. **18** (2000) 185.
[22] J. Simonin, Chem. Eng. J. **300** (2016) 254.
[23] Y. Cai, X. Zhu, W. Hu, C. Zheng, Y. Yang, M. Chen, X. Gao, J. Ind. Eng. Chem. **70** (2019) 447.
[24] H. Tavakkoli, F. Hamedi, Res. Chem. Intermed. **42** (2016) 3005.
[25] S. Lan, L. Liu, R. Li, Z. Leng, S. Gan, Ind. Eng. Chem. Res. **53** (2014) 3131.
[26] Y. Li, A. Meas, S. Shan, R. Yan, X. Gai, Bioresour. Technol. **207** (2016) 379.
[27] L. Wang, J. Li, Y. Wang, L. Zhao, J. Hazard. Mater. **196** (2011) 342.
[28] G.C. Panda, S.K. Das, A.K. Guha, J. Hazard. Mater. **164** (2009) 374.
[29] G. Germinario, E.C.L. Rigante, I.D.V. Werf, L. Sabbatini, J. Anal. Appl. Pyrolysis **127** (2017) 229.
(Rec. 09/02/2021, Rev. 28/04/2021, Ac. 26/05/2021)